Study of multivacancies in alpha Fe

Dmytro Kandaskalov, Claude Mijoule, Damien Connétable *

CIRIMAT UMR 5085, CNRS-INP-UPS, École Nationale d'Ingénieurs en Arts Chimiques et Technologiques (ENSIACET) 4, allée Émile Monso, BP 44362, F-31030 Toulouse Cedex 4, France

A B S T R A C T

Formation and migrations energies were calculated for multi-vacancies V_n (n = 1–15) in bcc Fe bulk and its surfaces using density functional theory. In this work, we analyze the evolution of the formation energy, the migration processes and the stable configurations of V_n. For small clusters (mono- and divacancies), our results are in agreement with those from the literature. We also focused on the study of the interactions between surfaces (Fe(1 0 0) and Fe(1 1 0)) and a vacancy, which enabled an assessment of the interactions the between vacancy and free surfaces. For V_3, we found that the more compact structure (labeled (1 1 2)) is a more stable configuration than that of V_4 (1 1 1 1 2 2). The migration mechanisms of V_2 and V_3 are decomposed to identify the position of the transition states, and to thus explain the low migration energy of V_3. An analysis of the structure of different clusters shows that for $n \leqslant 10$, the more stable structures are built from 2NN and 1NN divacancies. We suggest some stable compact configurations for large clusters.

1. Introduction

Defects, such as vacancies, cavities or grain boundaries, have a considerable impact on the physical and technological properties of metals such the embrittlement, strengthening, crack resistance, ductility or creep behaviors [1], and can lead to premature aging in structures. The irradiation of nuclear materials is a classical example. Irradiation by electrons [2], ions [3,4] or neutrons [5,6] is the most common method for point defect production. The generation of supersaturated vacancies can also be observed for quenching from high temperatures [7–9], high speed or heavy plastic deformations [10] and even oxidation [11]. It was observed that metals with different crystal lattices, bcc [12], fcc [13], or hcp [14], have different propensities towards the formation of the cavities mentioned above [15]. Obtaining knowledge on the properties of the point defects and their precipitations (cavities or precipitates) is the focus of many theoretical and experimental works.

Point defect reactions that are related to point defect cluster formation have been reviewed for different types of crystallographic structures for metals and for a wide variety of experimental treatments [15]. However, a main dependence of the formation of any type of cluster on the metal has not been found, and only correlations were observed [15]. Despite the various wide physical properties that have been used to study vacancy formation and migration, such as enthalpy, specific heat, thermal expansion, electrical resistivity, thermopower, positron annihilation and the perturbed angular correlation of gamma quanta [16], the process of cavity formation is not sufficiently clear. The theoretical study of vacancies and cavities is a good addition to experimental studies to obtain a better understanding of cluster formation.

In our work, we focus on iron, which is a main component of the ferritic and austenitic steel structural alloys and of some other structural alloys. Structural alloys that are used in high-temperature applications exhibit complex thermo-mechanical behavior that is time dependent and hereditary. The main application of these steels is in aeronautic and nuclear materials devices. Ferritic steels are used for their combination of high strength, high toughness, and corrosion resistance, as well as their combination of low cost, weldability, strength and corrosion resistance when alloyed with sufficient amounts of Cr. The knowledge of materials in which some small cavities could appear is thus of great technological interest.

The purpose of this work is to analyze the evolution of the formation energies and the migration processes of clusters. The layout of this paper is as follows: in Section 2, we present our DFT computational framework. We then present the results of the formation and migration of a monovacancy in the bulk (Section 3). Section 4 is devoted to the results of the excess energies of the Fe(1 0 0) and Fe(1 1 0) surfaces and of the formation energies of monovacancies on and near the surfaces. In Sections 5–7, the results of the formation of V_n-vacancies (n = 2–4) in the bulk using DFT calculations are presented. We then present the larger multivacancies V_{5-10} and V_{11-15} in Section 8. We conclude by analyzing some large clusters in Section 9.

* Corresponding author. Tel.: +33 5 34 32 34 10.

E-mail addresses: dmytro.kandaskalov@ensiacet.fr (D. Kandaskalov), damien.connetable@ensiacet.fr (D. Connétable).

2. Methodology

2.1. Theoretical method of calculations

Our calculations were performed using the Vienna *ab initio* simulation package (VASP) [17]. Self consistent Kohn Sham equations were solved using the projected-augmented wave (PAW) method [18] to describe the electron–ion interactions and the Perdew–Wang approximation (PW 91) [19] for the exchange and correlation functionals. The spin effects are taken into account in all calculations. The plane-wave energy cut-off was fixed at 400 eV, and $4 \times 4 \times 4$ Monkhorst–Pack meshes [20] were used to sample the Brillouin zone for large supercells (128 and 250 atoms [21]). The energy does not vary by more than 1 meV/atom for these criteria. Lattice relaxations were introduced by using a conjugate-gradient algorithm. Ions and lattice parameters were allowed to relax.

Fe(110) and Fe(100) surfaces were designed using slabs and were composed of 12 atomic layers. To separate the vacancies from the neighboring supercells, we used a "c(2×2)" (centered 2×2) supercell for the Fe(110) surface and a "p(3×3)" (primitive cell 3×3) for the Fe(100) surface. In both cases, symmetric slabs were used and the calculations were done with $7 \times 7 \times 1$ k-meshes. The surface energies, inter-layer distances and inter-layer forces were taken as convergence criteria to choose the optimal number of layers for each part of the slab. To avoid an artificial dipole moment on the surface, we introduced one vacancy on both sides of the slab. We optimized the vacuum (the number of empty slab) that separates the metal layers: for the Fe(110) and Fe(100) surfaces, we used 5 layers (d = 12.7 Å) and 8 layers (d = 12.0 Å), similar to in previous theoretical works [22,23]. The schematics of the structures that were used are reproduced in Fig. 1.

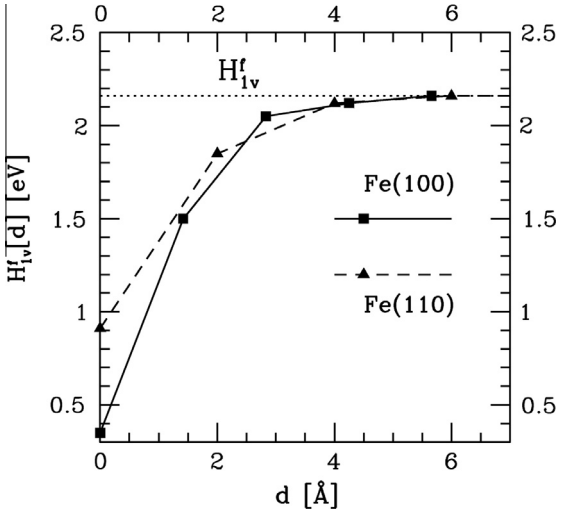

Fig. 2. Evolution of the formation energy of the vacancy according to the surface.

2.2. Thermodynamic properties of defects

The formation enthalpy of the n-vacancies (labeled V_n) is given by $H^f_{nv} = E^f_{nv} + p\Omega^f_{nv}$, where E^f_{nv} is the formation energy of V_n, Ω^f_{nv} is the formation volume and p is the pressure. In the following H^f_{nv} is labeled as E^f_{nv}, the pressure effects are neglected. The volume of the unit cells is relaxed.

Assuming that N is the number of Fe atoms in the super-cell, the enthalpy of formation of a cluster (E^f_{nv}) is expressed as:

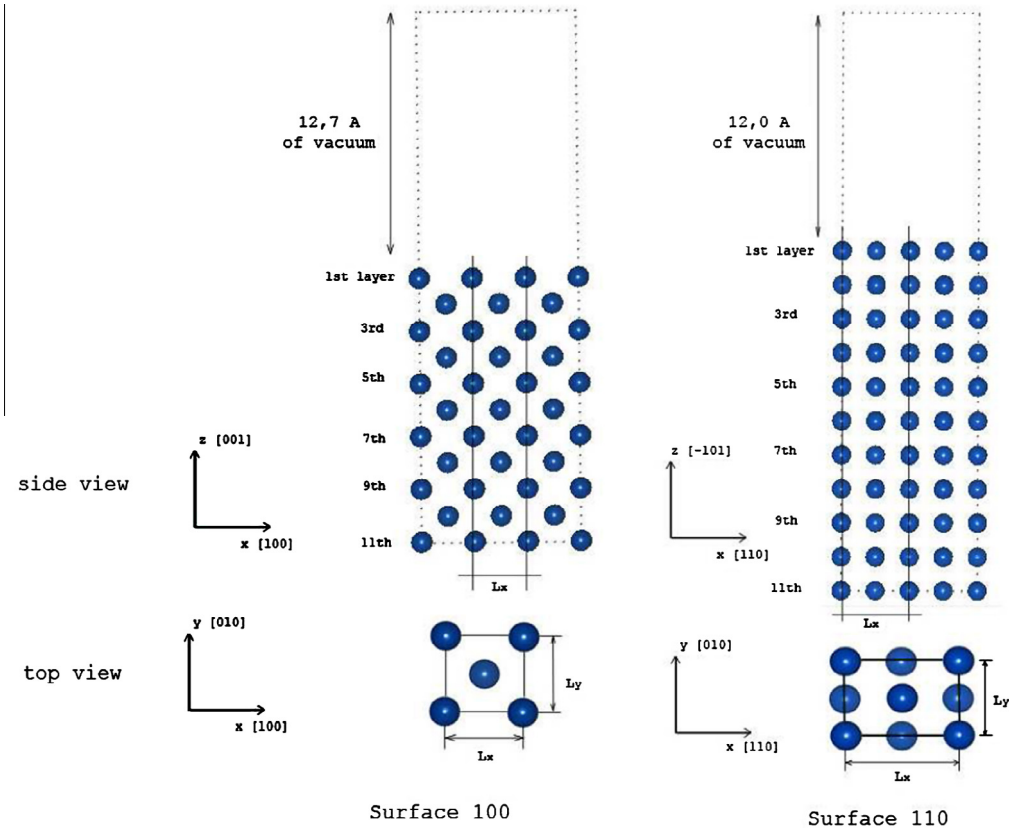

Fig. 1. Schematics of the Fe(100) and Fe(110) surfaces of size p(3×3) and c(2×2) respectively.

$$H^f_{nv} = E_o(n, V_n) - \frac{N-n}{N} \cdot E_o(0, V_o) \quad (1)$$

where $E_o(n, V_n)$ is the total energy of the super-cell with a relaxed unit cell volume (V_n), which contains N–n atoms of iron and n monovacancies. $E_f(0, V_o)$ is associated with the total energy of the supercell that has N atoms and a relaxed unit cell volume of V_o. In the following, we introduce the formation energy per monovacancy $\left(E^f_{nv}/n\right)$ for a better understanding of and comparison between the results.

The migration enthalpy of the mono- and divacancies $\left(E^m_{1v/2v}\right)$ is expressed by:

$$H^m_{nv} = E^{sp}_{nv} - E^f_{n,V_n} \quad (2)$$

where E^{sp}_{nv} is the energy of the saddle point. To characterize a cluster of size n, two additional energies are defined: the trapping energy (E^t_{nv})

$$E^t_{nv} = E^f_{(n-1)v} + E^f_{1v} - E^f_{nv} \quad (3)$$

which corresponds to the ability of a V_{n-1} to capture an nth vacancy, and the binding energy $\left(E^b_{nv}\right)$:

$$E^b_{nv} = nE^f_{1v} - E^f_{nv} \quad (4)$$

which corresponds to the excess energy. A positive binding energy means that the V_n defect is more stable than n isolated monovacancies.

The formation energy of a vacancy E^f_{1v} on a symmetric surface is calculated by the following expression:

$$E^f_{1v}(surf) = \frac{1}{2}(E_{slab}[(N-2)\cdot \mathrm{Fe}] - E_{slab}[N \cdot \mathrm{Fe}] - 2E_{atom}) \quad (5)$$

where $E_{slab}[N\cdot\mathrm{Fe}]$ and $E_{slab}[(N-2)\cdot \mathrm{Fe}]$ are the total energies of the relaxed slab without and with a vacancy on each side of the slab, respectively. E_{atom} is the atom energy of Fe in the bulk.

3. Monovacancy in the bulk

3.1. Formation energy of the monovacancy

We list experimental and theoretical data from the literature in Table 1. Experimentally, the formation energy of the monovacancy has been measured to be between 1.4 and 2.0 eV, while the theoretical values (LDA and GGA) overestimate this energy (1.95–2.17 eV). The model that is based on surface intrinsic errors suggests that the theoretical values should increase up to 2.32–2.71 eV [24], which increases the disagreement between theory and experiment.

Our value (2.16 eV, obtained with a $4 \times 4 \times 4$ supercell) is consistent with the theoretical results from the literature. The formation volume of the monovacancy $\left(\Omega^f_{1v}\right)$ is found to be approximately 7.43 Å^3, i.e., $\Omega^f_{1v} \simeq 0.65\Omega_o$ (where Ω_o is the atomic volume for the equilibrium lattice parameters without the vacancy), which is in agreement with the expected volume for bcc metals [38].

Within the quasi-harmonic approximation, the vibrational free energy correction (F_{vib}) of the monovacancy at 0 K (zero point energy, calculated with a $3 \times 3 \times 3$ supercell at the Γ point) is given by:

$$F_{vib} = E_{vib}[(N-1)\cdot \mathrm{Fe}] - \frac{N-1}{N} \cdot E_{vib}[N \cdot \mathrm{Fe}] \quad (6)$$

where $E_{vib}[X] = \sum \hbar\omega_{q=\Gamma,v}[X]/2$ is the vibrational energy calculated with and without the vacancy. The ZPE is found to be small, approximately −10 meV. This value is too low to significantly modify the formation enthalpy of the monovacancy.

Finally, we calculated the formation entropy $\left(S^f_{1v}\right)$ which relies on the derivation of the vibrational free energy $S = -\frac{\partial F_{vib}}{\partial T}$. In the limit ($T \to \infty$), we have:

$$S^f_{1v} = S^{1v} - \frac{N-1}{N} S^{bulk} \simeq k_B \left[\left(\frac{N-1}{N}\right) \sum_{m=1}^{3(N-1)} \ln\left(\omega^{bulk}_m\right) - \sum_{m=1}^{3(N-2)} \ln\left(\omega^{1v}_m\right) \right] \quad (7)$$

We obtained approximately 0.8 k_B for S^f_{1v}; previous estimations [39–41] gave 1–2 k_B. Lucas and Schaeublin [42] obtained 4 k_B using an equivalent approach without cell relaxation. It must be noted that the formation entropy is sensitive to the values of the frequencies (and thus to the relaxation of the cell), and a large volume induces an increase in entropy. Using the same methodology as [42], we obtain 3 k_B.

3.2. Migration of the monovacancy

To complete the study of the monovacancy properties, we present its migration process. The diffusion coefficient of the monovacancy is given by:

$$D_{1v} = D_o \exp\left[-\frac{E^m_{1v}}{k_B T}\right] \quad (8)$$

where E^m_{1v} is the migration energy, $D_o = a_o^2 v_o$, v_o is the attempt frequency and a_o is the lattice parameter of the unit cell. In this case, the migration process corresponds to the displacement of one Fe atom along the ⟨1 1 1⟩ direction. The migration along the ⟨1 0 0⟩ axis is energetically unlikely because of a high barrier (approximately 2.5 eV). The Fe atom needs to cross a square of Fe atoms that is located in the middle of the path.

In the direct migration path, there are 3 barriers (labeled 3-6-3): 2 identical 3-coordinated sites that are located one third and two thirds of the way along the migration path and a 6-coordinated site midway along the path. For the two configurations, we found energies of 0.54 and 0.64 eV. The migration saddle point (with a migration energy of 0.64 eV) is located at the center of the path. This value is in excellent agreement with experimental data (0.55 eV [43] was measured for a high-purity α-Fe) and with previous theoretical works (0.65–0.67 eV [28,44]). Fu [44] also obtained (using NEB calculations, see Fig. 3a in Ref. [44]) equivalent values: 0.54 eV for the 3-coordinated sites and 0.64 for the saddle point.

The jump frequency (v_o) can be evaluated using only a first-order approximation of the Vineyard theory [45]: $v_o = \prod_{i=1}^{3N-3}\omega_i / \prod_{i=1}^{3N-4}\omega_i^*$, where ω_i and ω_i^* are the *eigen-frequencies*

Table 1
Formation energies (E^f_{1v}, in eV) of the monovacancy, comparison between theory and experimental data.

Theo.		Exp.
US–GGA	2.04 [25]	
LSGF-LDA	2.25 [26]	1.5 ± 0.1[a]
FPLMTO–LDA	2.18 [27]	1.60 ± 0.15[a]
US–GGA (PW 92)	1.95 [28]	1.40 ± 0.1[b]
PAW–GGA	2.15 [29]	2.0 ± 0.2[c]
EAM	1.73 [25]	1.81 ± 0.1[d]
US–GGA (PW91)	2.09 [28]	2.0[e]
US–GGA (PW91)	2.02 [29]	
SIESTA–GGA (PBE)	2.07 [30]	
PAW–GGA (PBE)	2.17 [31]	
Present Work PAW–GGA (PW91)	2.16	

[a] Wing parameter in Doppler broadening, Refs. [32,33].
[b] Normalized peak counting rate in angular correlation, Refs. [34,35].
[c] S parameter in Doppler broadening, Ref. [36].
[d] Positron life time spectroscopy, Ref. [37].
[e] Doppler boarding at low temperature, Ref. [36].

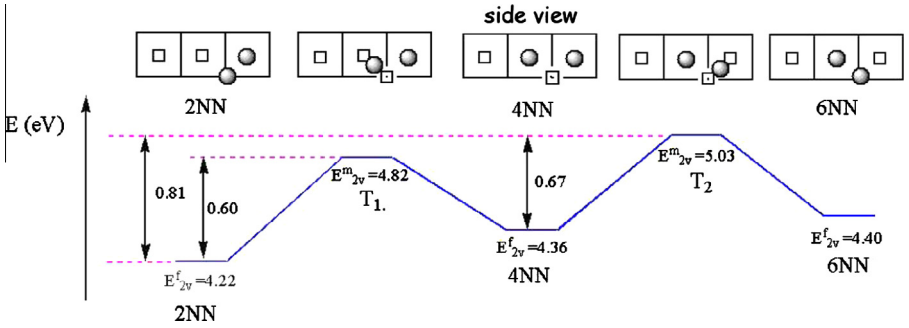

Fig. 3. Indirect migration path, 2NN towards 6NN.

of the equilibrium configuration (with the vacancy) and the migration state, respectively. The attempt frequency is approximately 844 THz, which gives $\simeq$0.68 cm^2/s for D_o. Our diffusion constant D_o is slightly greater than those in previous works, 0.16 cm^2/s for Hatcher et al. [40] and 0.001 cm^2/s for Osetsky and Serra [46], but is in better agreement with experimental data, 1.0 cm^2/s (see Ref. [40]).

4. Vacancies on Fe(100) and Fe(110) surfaces

4.1. Fe(100) and Fe(110) surface energies

The effect of a free interface on the monovacancy formation energy was analyzed using a study of Fe surfaces. We first computed the surface energies of Fe(100) and Fe(110) surfaces using the following approach:

$$\gamma_{surf} = \frac{1}{2}(E_{slab} - nE_{layer}) \tag{9}$$

where E_{slab} is the total energy of the slab, E_{layer} the total energy of the layer in the bulk crystal and n is the number of bcc layers in the slab.

As pointed out by Boettger [47], to obtain a converged surface energy for a slab with varying thickness, it is crucial to ensure that E_{layer} is consistent with the large n limit of the incremental energy difference for the slab. E_{layer} can be accurately determined from the linear plot of E_{slab} vs n. The intersection of this plot with the y-axis gives the double surface energy, and the slope ratio gives an accurate value for E_{layer}.

We obtained 2.45 and 2.58 J/m^2 (0.86 and 1.29 eV/atom) for Fe(110) and Fe(100) respectively (using a linear fit). We note that our results are in excellent agreement with previous theoretical works 2.26–2.66 J/m^2 for Fe(110) and 2.22–2.48 J/m^2 for Fe(100) [48–52]. The experimental data that was obtained for polycrystalline surfaces, is approximately 2.41–2.55 J/m^2 [53,54]. With good approximation, we use these data for comparison with the theoretical results of low indexed surfaces. Low indexed surfaces have approximately the same surface energy [48].

These excess energies correspond to the limiting case of the surface energies of large clusters. For a cavity, one of the physically relevant variables is the energy per unit area or per atom on the surface ($E^{surface}_{cavity}$). We need to obtain an expression in accordance with the topology of the cavity: $E^{surface}_{cavity} = f(\gamma_{110}, \gamma_{100})$. For example in the case of the cubic V_9 defect (see below), the cavity is composed only of Fe(100) surfaces.

4.2. Formation energy of the monovacancy on Fe(100) and Fe(110) surfaces

Using the optimized geometry described above, we study the stability of one monovacancy near free interfaces (with a supercell approach). The choice of simulation boxes corresponds to a vacancy coverage of approximately 0.111 and 0.125 (for Fe(100) and Fe(110) surfaces, respectively), which is low enough to neglect in a first-order approximation of the vacancy–vacancy interactions. To quantify the effect of the surface density on the vacancy formation energy, we used larger supercells (in the x–y plan): p(4 × 4) and c(3 × 3) surfaces [55]. It thus corresponds to surface densities of 6.3% and 5.5% (the results are labeled †).

The vacancy formation energies on the Fe(110) and Fe(100) surfaces are found to be 0.91/0.96† and 0.35/0.30† eV, respectively. Wang et al. [56,57], using EAM methods, found approximately 0.70 and 0.58 eV, in agreement with our results. These values are significant lower than that in the bulk (2.16 eV), which can be linked to dangling bonds into the surfaces.

The supercells contain 9/16† and 8/18† Fe atoms per surface (for the Fe(100) and Fe(110) surfaces, respectively), the surface per atom are thus equal to approximately 8.1 and 5.7 Å^2/atom (see Table 2). The freed surface, by the monovacancy, is dependent of the surface. We obtain a slight evolution of H^f_{1v} according to the vacancy density (from high to low densities): H^f_{1v} decreases in the case of low indexes surfaces and increases in the case of dense surfaces.

We then studied the evolution of this formation energy as a function of its position and the surface. Our results and those of Wang et al. [56,57] are listed in Table 3 and shown Fig. 2. We note that from the fourth (for Fe(110)) and fifth (for Fe(100)) atomic layer, the surface effects become negligible and the formation energies approach the formation energy of the bulk. Thus, we can generalize that the interaction of vacancy with a surface directly depends on the vacancy-surface distance and this interaction was completely negligible at a distance of 6 Å. The changing tendency the vacancy formation energy for the atomic layers of Fe(110) corresponds well with the results of Wang et al. [56].

5. Divacancies

5.1. Stability of divacancies

Different divacancy configurations were investigated from the first nearest neighboring configuration (labeled 1NN) up to the 7th nearest neighbor (7NN) configuration. The results are summarized in Table 4. Beeler and Johnson [58] reported that 2NN is higher in energy than the other divacancies (with a binding

Table 2
Correlation between the surface area per atom (measured in Å^2/atom), the number of atoms per surface, and the formation energies of the monovacancy according to the surface type (H^f_{1v}), measured in eV.

Surface		nb Atoms	Area/atom	Density	H^f_{1v}
Fe(100)	p(3 × 3)	9	8.1	11.1	0.35
	p(4 × 4)	16		6.3	0.30
Fe(110)	c(2 × 2)	8	5.7	12.5	0.91
	c(3 × 3)	18		5.5	0.96

Table 3
Formation energies of the monovacancy from the bulk through the surface (H^f_{1v}), in eV.

Position	Fe(100)		Fe(110)	
		Wang et al. [56]		Wang et al. [57]
Surface	0.35	0.58	0.91	0.70
2	1.50		1.85	1.65
3	2.05		2.12	1.84
4	2.12		2.16	1.86
5	2.16		2.16	1.86
bulk	2.16	1.86	2.16	1.86

energy of approximately 0.195 eV), while 1NN is lower in energy (approximately 0.131 eV). Masuda [59] showed that, for a divacancy, the relaxation of atoms plays a significant role in the relative stability of the 1NN and 2NN divacancies. For atomic relaxation, the authors found that both configurations have positive binding energies and that configuration 2NN is more stable than 1NN (0.01 eV). Jonhson and Oh [60] obtained, using EAM simulations, binding energies of approximately 0.16 and 0.22 eV for 1NN and 2NN, respectively. DFT calculations [25,28,31,61,62] give results that are close to those from the EAM calculations. Both pseudo-potentials (USPP and PAW) yielded equivalent binding energies for divacancy 1NN, while the USPP led to a larger stability for 2NN [28,61]. USPP gives the relative difference in stability between 2NN and 1NN as 0.14 eV, while PAW gives 0.01–0.06 eV. However, Fu et al. [44] found a higher binding energy (0.3 eV) for 2NN, which could be explained by the method the authors used in their work (SIESTA code, with Troullier–Martins pseudo-potentials).

Our calculations (given either for a constant volume – urlx – or for a constant pressure – rlx) confirm that 2NN should be more stable than the other divacancies ($E^f_{2v} = 4.126$ eV). However, the 2NN binding energy is very close to that of 1NN, approximately 10 meV different. The other divacancies (from 3NN to 7NN) have binding energies close to zero. For 3NN the binding energy is negative (∼30 meV) and for 4NN and 5NN this energy is positive. For the 6NN configuration, the vacancies are not bound. The configuration (3NN) in which the two vacancies are along the ⟨1 1 0⟩ direction has a repulsive character.

We calculated the formation volumes Ω^f_{2v} of the divacancies. These volumes are in the range of 0.64–0.69Ω_o, which is close to the formation volume of the monovacancy. No correlation between the stability of the divacancy and the formation volume has been found.

5.2. Migration of 2NN

To move without being dissociated, 2NN should have the 1NN divacancy as a transition state. The lowest-energy path – from 1NN to 2NN – leads to a transition state, that is located 2/3 of the way along the Fe-atom migration path with a 0.55 eV migration energy. Because there is an additional vacancy in comparison with the monovacancy, the migration path is referred to as "2-5-3". The highest barrier is for the 3-coordinated site, which is the same site as for the monovacancy that was presented above. For the divacancy, the migration energy through the 5-coordinated site is 0.50 eV.

We can now compare our results with those of the literature. We note that Fu et al. [44] obtained a migration energy of 0.62 eV (0.52 eV for the reverse migration), and that Djurabekova et al. [61] obtained 0.66 eV (0.60 eV for the inverse migration) which are slightly higher than our values (0.55 eV and 0.54 eV). The main difference between our results and those of Fu can be explained by the relative stability of 2NN in comparison with 1NN in our simulations and theirs. The difference with the Djurabekova results remains unclear (the same approach as ours was used). The difference with our value can be explained by the approximations used in their simulations: the "Vosko Wilk Nusair" correction, 300 eV for the cut-off energy, and the reciprocal space of their supercells (128 atoms) has been sampled with 27 k-points.

5.3. Formation and dissociation mechanisms of the divacancy

To complete the description of divacancies, we studied the formation–dissociation mechanisms of the divacancies along two directions: along the ⟨1 1 1⟩ direction (from 1NN to 5NN) and along the ⟨1 0 0⟩ direction (from 2NN to 6NN).

In the first case, the barriers are approximately 0.64 and 0.53 eV for the dissociation and formation mechanisms, respectively. This case is similar to the migration of the monovacancy along the 3-6-3 path with the saddle point at the center.

For the second migration mechanism, as was expected, the energy of the saddle point is unfavorable: 2.49 and 2.31 eV for the dissociation and formation barriers of 2NN, respectively. We thus investigated an indirect mechanism: a migration through the 4NN divacancy (as illustrated in Fig. 3). In this case, two transition states, T_1 (E^m = 4.82 eV) and T_2 (E^m = 5.03 eV), are necessary. The lowest barrier of 2NN towards 6NN is reduced to 0.60 and 0.67 eV for dissociation and formation, respectively. The results, which are summarized in Table 5, are in agreement with those of Beeler and Johnson [58].

The most surprising result is that the migration–formation energies of the divacancy and of the monovacancy are very close. These results also show that the migration energies of the monovacancy are slightly dependent on the vacancy–vacancy distance and are approximately 0.55–0.70 eV.

6. Trivacancies

6.1. Stability

We use the common nomenclature to describe the trivacancies: three integer numbers (labeled *lmn*) that characterize the pairwise

Table 4
Formation volume (Ω^{2v}_f, in Ω^{2v}_o units) and formation (E^f_{2v}, in eV) and binding (E^b_{2v}, in eV) energies of the divacancies.

	Ω^{2v}_f	E^f_{2v}	E^b_{2v}	E^b_{2v}						
	This work			[58]	[59]	[61]	[25]	[28]	[31]	[62]
1NN	0.681	4.226/4.136[a]	0.174/0.184[a]	0.131	0.044	0.17	0.17	0.15	0.16	0.17
2NN	0.669	4.215/4.126[a]	0.184/0.194[a]	0.195	0.054	0.23	0.23	0.29	0.23	0.19
3NN	0.641	4.406/4.351[a]	−0.005/−0.031[a]	−0.03						
4NN	0.668	4.358/4.265[a]	0.042/0.055[a]	−0.05		0.03				
5NN	0.685	4.344/4.255[a]	0.056/0.065[a]	−0.01		0.05				
6NN[b]	0.670	4.409/4.323[a]	−0.009/−0.003[a]	−0.03						
7NN[b]	0.671	4.400/4.319[a]	0.000/0.001[a]							

[a] Unrelaxed/relaxed supercell.
[b] Calculations were done with large supercells (250 atoms).

Table 5
Migration energies for different migration paths (dissociation and formation energy paths, in eV); D = dissociation and F = formation.

	Our results		Djurabekova et al. [61]		Beeler and Johnson [58]	
	D	F	D	F	D	F
1NN–5NN	0.64	0.53	0.74	0.62	0.72	0.57
2NN–6NN	2.49	2.31	–	–	–	–
2NN–1NN	0.60	0.46	0.66	0.46	0.65	0.50
4NN–6NN	0.67	0.63	–	–	0.75	0.73

nearness of the vacancies. For example, the (112) configuration is composed of two 1NN and one 2NN (see Fig. 4). This nomenclature will be used to describe larger multivacancies.

We limited our study of trivacancies to seven compact configurations (shown in Fig. 4): (112), (223), (235), (226), (115), (113) and (124). Our results, those of Beeler and Johnson [58] and those of Masuda [59] are reported in Table 6. The reference state of the divacancies was 2NN to compute the trapping energy of V_3 (E^t_{3v}).

The most stable configuration is the (112) compact configuration with a formation energy (E^f_{3v}) of 5.97 eV, in agreement with previous theoretical works. The two linear three-vacancies (226) and (115) and the three-vacancy (124) have close formation energies (6.20–6.22 eV). The three configurations that have 3NN blocks (the (113), (235) and (223) clusters) are the most unstable defects. We can relate this result to the unstable nature of the 3NN divacancy (see Table 4); 1NN and 2NN blocks appear to stabilize V_3, contrary to 3NN. We can also note that the (226) and (115) configurations, which are derived from 2NN and 1NN,respectively, have the same difference in their formation energies as divacancies 2NN and 1NN. This result can also be explained by the pairwise link, in which 2NN and 5NN are more stable than 1NN and 6NN, respectively. These conclusions will be used to interpret larger V_n.

6.2. Migration of the V_3 (112)

The study of the migration of the most stable V_3 (112) is especially interesting because there are two different sets of theoretical results: the set from Beeler, who obtained 0.66 eV, which is equivalent to the migration energy of the monovacancy, and the set of Fu et al. [44], who used an NEB method and obtained an energy of 0.35 eV. Fu does not explain why the migration of the V_3 (112) is significantly smaller than the previous result. For both results, the transition state is located in the middle of the migration path. Beeler fixed the transition state exactly between two vacancies, while, in the NEB calculations the atom can freely move in the transition state, which was not described by Fu et al. [44].

We report the results of two types of numerical simulations: either we fixed the Fe atom between the two nearest vacancies or we put it in the center of a four-vacancy (see Fig. 5). In the first case, we obtained 0.64 eV, which corresponds well to the results of Beeler, and, in the second simulation, we obtained 0.36 eV, which corresponds well to the results of Fu. The migration path for V_3 can thus be labeled as 2-4-2 in which the transition state is 4-coordinated and located at the center. The transition state is located at the center of the fourth vacancy V_4, and n equivalent result was obtained for the diffusion of V_2 in hcp-Ti[63]. The migration state can be viewed as an auto-interstitial inside a V_4.

We can therefore assume some general trends for the migration: through a 6-coordinated state, the migration energy should be approximately 0.64 eV (V_1), through a 5-coordinated state (V_2), it should be 0.50 eV and, through a 4-coordinated state (V_3), it should be 0.36 eV. Moreover, we note that the migration energy decreases from the monovacancy until V_3.

7. V_4 multivacancies

7.1. Stability

To study V_4, we took into consideration six configurations (shown in Fig. 6): (111122), (111223), (111333), (111224), (222333) and (222233). These configurations can be compared with those of Beeler and Masuda [58,59]. The formation, binding and trapping energies are listed in Table 7. The stability remains the same as that for V_3: the V_4 multivacancies that are composed of a large number of 1NN and/or 2NN blocks are more stable than the other multivacancies. The most stable structure is (111122), the tetrahedral configuration. We then obtain the (111223) and (111224) configurations. Beeler found that (111223) is more stable than (11124). When unit cell relaxations are involved, (111223) becomes energetically more stable than the other multivacancies (see Table 7).

For the (222333) and (223333) structures, we obtain negative trapping energies. Masuda obtained a binding energy of close to zero for (223333). From the rapping energies, a slight instability in the (222333) and (223333) configurations could be noted, which suggests that it should not be possible to form these V_4 from the V_3 (112) cluster (the most stable trivacancy). In this case, we note that the stability of pairwise links plays a significant role in the stability of larger multivacancies, which explains the fact that (111122) is the most stable. We can also observe that Beeler's results for V_3 and V_4 multivacancies with 3NN motifs give binding and trapping energies that are relatively close to those with 1NN patterns. We can explain this result by the fact that 1NN

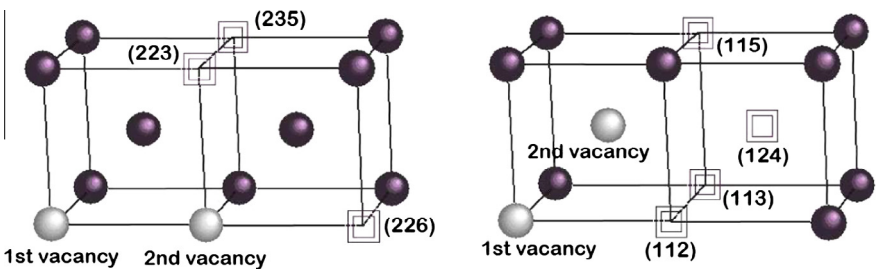

Fig. 4. Schematic of the studied trivacancies.

Table 6
Trapping energies (E^t_{3v}, in eV), binding energies (E^b_{3v}, in eV) and formation energies (E^f_{3v}, in eV) of trivacancies.

V_3	Ref. [58]		Ref. [59]	This work urlx/rlx		
	E^b_{3v}	E^t_{3v}	E^b_{3v}	E^f_{3v}	E^b_{3v}	E^t_{3v}
(112)	0.49	0.29	0.24	5.97/5.82	0.63/0.66	0.44/0.46
(223)	0.36	0.17	−0.02	6.72/6.70	−0.12/−0.22	−0.31/−0.41
(235)				6.36/6.21	0.24/0.27	0.05/0.07
(226)	0.39	0.19		6.21/6.13	0.39/0.35	0.20/0.15
(115)	0.27	0.14		6.22/6.15	0.38/0.33	0.19/0.13
(113)	0.25	0.12		6.27/6.14	0.32/0.34	0.14/0.14
(124)				6.20/6.08	0.40/0.40	0.21/0.20

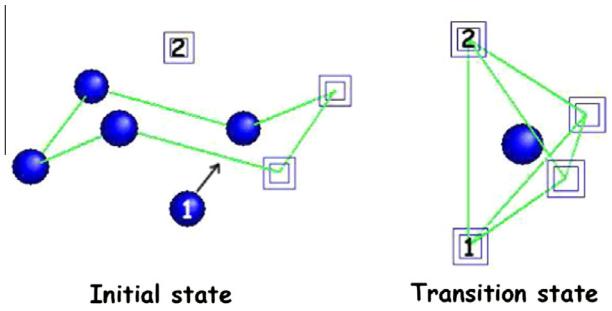

Fig. 5. Migration of the V_3(112): at left the initial state, and, at right, the transition state.

(E^b = 0.13 eV) is less stable in Beeler's case than in our case (E^b = 0.18 eV). Qualitatively, from these results, we can argue that the most compact configurations, which are composed of a larger number of 1NN and 2NN blocks, should be stable configurations.

From a formation point of view, the most stable V_{n+1} configuration should be formed directly from the most stable V_n. V_{n+1} should thus be composed of the most stable compact block V_n, i.e., composed of 1NN or 2NN. Beeler [58] found the same behavior for the stability of V_n using the fact that the (112) trivacancy should be a "flexible" block and can migrate without changing its configuration. V_3 should be considered an elementary brick for building larger V_n multivacancies.

7.2. Migration of (111122)

To move, the multivacancy V_4 (111122) should migrate through an intermediate state: (111223). For this mechanism, Fu obtained a barrier of 0.48 eV, which corresponds to a "2-4-2" type, similar to that of V_3 (see the migration mechanism in Fig. 5). The barrier should thus be equivalent to that of V_3. In our case the difference between both V_4 configurations is 0.16 eV.

Because the transition state is situated in the middle of the migration path, the contribution to the migration energy is 0.08 eV and the total energy of migration is 0.44 eV. Most of the bigger multivacancies have the 4-coordinated transition state. Thus, for these multivacancies, the expected migration is 0.36 eV with addition of the geometric contribution, so the initial and final states would be different.

8. Multivacancies V_{5-10}

For larger multivacancies (V_{5-10}), after studying different configurations, we found that the most stable structure should be composed of a large number of 1NN and 2NN patterns. A generalization can be proposed: the stable cavity should be viewed as a collection of 2NN blocks (see Fig. 7), which is a tendency that

Table 7
Trapping (E^t_{nv}, in eV), binding (E^b_{nv}, in eV) and formation energies (E^f_{nv}, in eV) of V_4.

V_4	Ref. [58]		Ref. [59]	This work urlx/rlx		
Structure	E^b_{nv}	E^t_{nv}	E^b_{3v}	E^f_{nv}	E^b_{nv}	E^t_{nv}
(111122)	1.02	0.53	0.66	7.43/7.33	1.37/1.31	0.73/0.66
(111224)	0.79	0.30	0.48	7.73/7.59	1.06/1.05	0.43/0.40
(111223)	0.84	0.36		7.74/7.49	1.08/1.15	0.44/0.49
(111333)				8.04/7.89	0.76/0.75	0.12/0.10
(222333)				8.20/8.05	0.60/0.59	−0.03/−0.07
(222233)	0.75	0.26	0.034	8.35/8.05	0.45/0.59	−0.18/−0.07

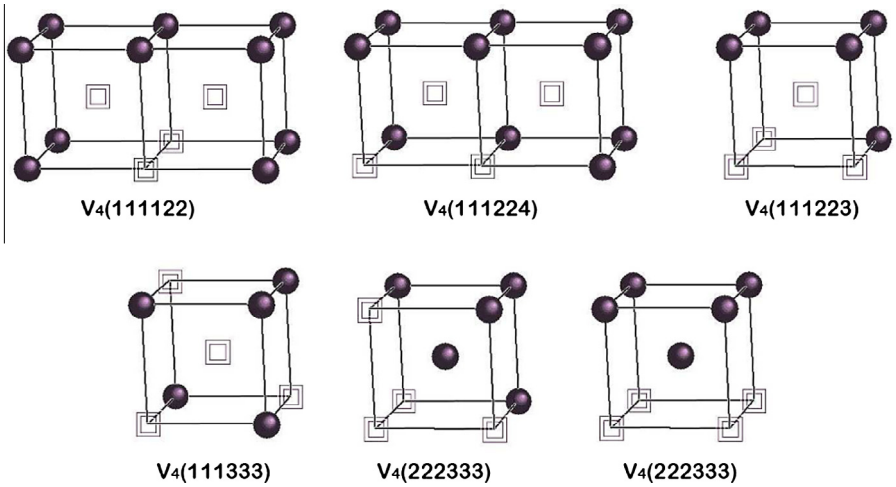

Fig. 6. Representation of V_4 multivacancies.

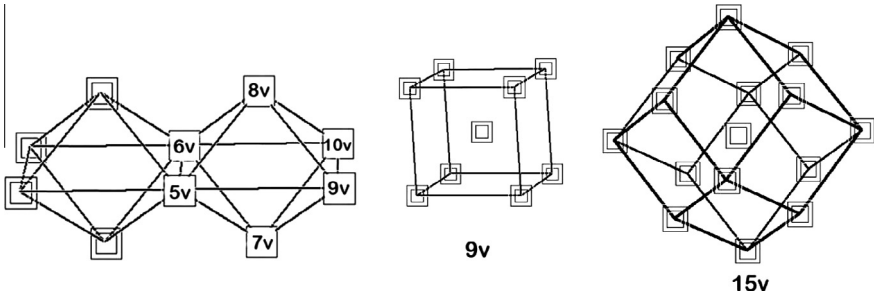

Fig. 7. V_{5-10} multivacancies that were considered (top) and formed from V_4 (the double square vacancy): the V_5–V_{10} (square vacancies), cubic V_9 and rhombo-dodecahedric V_{15} multivacancies.

Table 8
Formation, trapping and binding energies of V_n (in eV) according to n.

	V_5	V_6	V_7
E^f_{nv}	8.85/8.64	10.05/9.85	11.54/11.30
E^t_{nv}	0.78/0.80	0.98/0.95	0.71/0.71
E^b_{nv}	2.15/2.16	3.08/3.11	3.86/3.82
	V_8	V_9	V_{10}
E^f_{nv}	12.78/12.52	14.30/13.93	15.48/15.18
E^t_{nv}	0.96/ 0.94	0.68/0.75	1.02/0.91
E^b_{nv}	4.82/4.76	5.50/5.51	6.52/6.42

was already mentioned by Beeler [58]. In Table 8, we list the formation, binding and trapping energies of these V_n. We can notice oscillations in the trapping energy: between 0.71 and 0.95 eV. These oscillations can be explained by the parity of the multivacancies (the number of 2NN blocks): the multivacancies with an even number of vacancies are more stable than those with an odd number. This type of oscillations should be expected for larger cavities ($n > 10$) if the cavities are composed of 2NN.

The perpendicular growth of 2NN will be stable up to a given number n because, for larger number n, other possible configurations should exist. For this purpose, in the next section, we specially studied the stability of spherical multivacancies.

9. "Spherical" multivacancies V_{9-15}

For larger cavities, we then tried to identify a set of cavities that were more stable than previous cavities. We considered the "spherical" multivacancy family: the cubic V_9 and the rhombo-dodecahedric V_{15} (see Fig. 7). V_{15} is built from V_9 by removing 6 Fe atoms from each of the six cube sides. To verify our hypothesis, we considered all intermediate cases. In the case of V_{11} and V_{13}, we have two prospective configurations, as illustrated in Fig. 8. For example, V_{11} could have either the "together" or the "opposite" configurations. For both configurations, we obtained the same vacancy formation energy (within 20 meV).

We found (see Table 9) that the cubic V_9 is less stable than the V_9 that was built using 2NN blocks (see above). The cubic V_9 is composed of 12 3NN, which destabilize the defect. However, with the growth of the cubic V_9–V_{15}, the number of 1NN and 2NN grows more rapidly than the number of 3NN. The spherical multivacancies

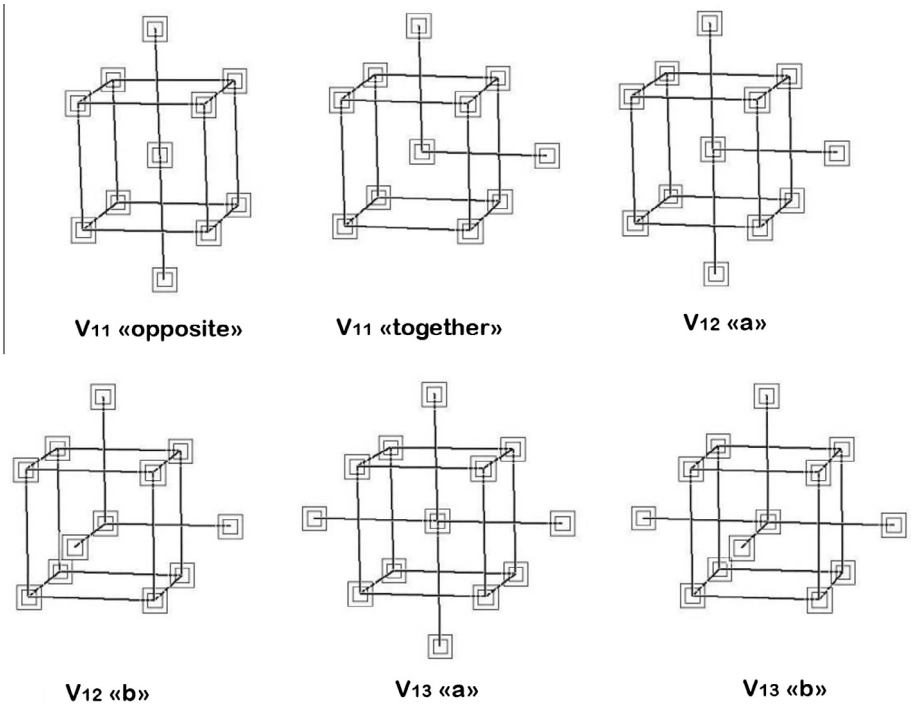

Fig. 8. Intermediate configurations.

Table 9
Comparison of the formation (E^f_{nv}, in eV) and trapping energies (E^t_{nv}, in eV) of V_9–V_{15}.

n	DFT (rlx)		
	E^f_{nv}	E^c_{nv}	E^t_{nv}
9	14.50	4.94	–
10	15.33	6.27	1.33
11a	16.09	7.67	1.39
11b	16.10	7.66	1.38
12a	16.96	8.96	1.29
12b	16.96	8.96	1.29
13a	17.69	10.39	1.47
13b	17.67	10.41	1.49
14	18.34	11.19	1.49
15	18.93	13.47	1.57

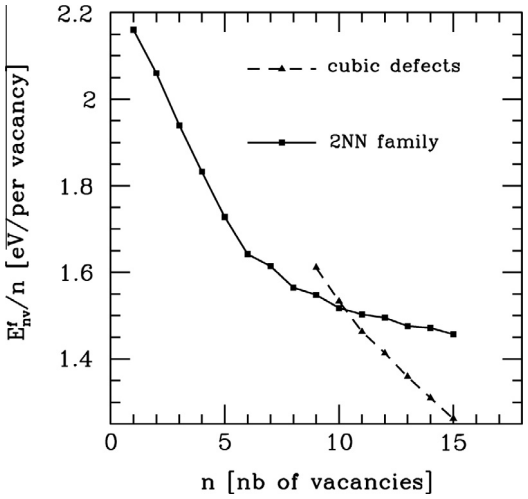

Fig. 9. Evolution of the formation energy per vacancy with the number of vacancies for different type of defects.

then become more stable than the previous family of multivacancies. This change was made from the "spherical" V_{11} defect.

We can see that the trapping energies for the growth of the spherical multivacancies (1.29–1.57 eV) are larger than those for the 2NN family (0.71–0.95 eV), indicating that the spherical vacancies should grow more easily. We can state the proposed formation of V_n from V_{n-1} more precisely: the most stable V_n can be formed from the most stable V_{n-1}, but there is a specific number n at which there is a complete geometric change in the configuration, as was shown above.

Fig. 9 shows the evolution of the V_n formation energy per vacancy for both types of V_n. For V_{1-6}, the energy decreases linearly and for V_{7-10}, there are small oscillations. Up to $n = 11$, the spherical defects become more stable.

10. Conclusion

In this work, we presented a study of the understanding of the structure and migration path of small cavities in bcc-Fe using DFT. These results should help to better understand the clusterization of V_n in iron using, for example, a general Ostwald ripening model. In summary, the main results that were presented in this manuscript are the following:

1. A detailed study of the monovacancy properties is presented from an energetic and a migration point of view. We obtained a formation energy of approximately 2.16 eV, a formation entropy of 0.8 k_B and a low ZPE correction (approximately 9 meV). The monovacancy migration energy and the diffusion coefficient are 0.64 eV and 0.68 cm^2/s, respectively. These results are in agreement with the literature.
2. The formation energy of the monovacancy on surfaces is given and discussed. We looked at the effect of these free interfaces on the monovacancy stability. Fe(100) and Fe(110) surfaces were considered. We show that it is easier to form a vacancy on a Fe(100) surface than on a Fe(110) surface. From the fourth layer, the proprieties of the vacancy are the same as those of the bulk. Near the surface energy γ, the properties should correspond to those of a large surface (a tension surface).
3. The study of divacancies shows that the 2NN and 1NN configurations are the most stable defects, with a small difference in their formation energy (approximately 10 meV), an that the V–V interactions quickly decrease (from 6NN). The migration of 2NN through 1NN is discussed in detail, and we note that the saddle point and the intermediate configurations in the migration mechanism could help in understanding larger V_n.
4. V_{3-4} multivacancies are also discussed from an energetic and migration point of view. These results indicate that the most stable configurations are obtained when the clusters are composed of a maximum number of 1NN and 2NN blocks. Moreover, we clearly identified the transitions states in their migration path. These defects appear to migrate with a lower energy than mono- or divacancies.
5. For V_{5-10}, we found that the most stable configurations are those that are composed of a perpendicular collection of 2NN blocks. Contrary to the previous results of Beeler, we showed that the V_n energy does not grow linearly.
6. Finally, the study of symmetric faults V_{9-15} shows that, from $n = 11$, there is a change in the stability of the different families: from the 2NN family to symmetrical defects.

Acknowledgments

This work was granted access to the HPC resources of *CALMIP* (CICT Toulouse, France) under the allocation 2010-p0912 and 2011/2012-p0850. DC acknowledges the support of the French Agence Nationale de la Recherche (ANR), under grant *EcHyDNA* (Blanc 10-19424). We also thanks Prof. D. Monceau for fruitful discussions and contribution.

References

[1] M.E. Kassner, T.A. Hayes, Int. J. Plast. 19 (2003) 1715–1748.
[2] M. Kiritani, Ultramicroscopy 39 (1991) 135.
[3] R. Schumacher, R. Vianden, Phys. Rev. B 36 (1987) 8258.
[4] K. Arakawa, R. Imamura, K. Ohota, K. Ono, J. Appl. Phys. 89 (2001) 4752.
[5] M. Kiritani, N. Yoshida, S. Ishino, J. Nucl. Mater. 602 (1984) 122–123.
[6] M. Kiritani, J. Nucl. Mater. 216 (1994) 220.
[7] P.B. Hirsch, J. Silcox, R.E. Smallman, K.H. Westmacott, Philos. Mag. 3 (1958) 897.
[8] D. Kuhlmann-Wilsdorf, H.G.F. Wilsdorf, J. Appl. Phys. 31 (1960) 516.
[9] M. Kiritani, J. Phys. Soc. Jpn. 19 (1964) 618.
[10] J. Philibert, A. Vignes, Y. Bechet, P. Comrad, Metallurgie du minerai au matriau Edition Masson, 1998.
[11] S. Perusin, B. Viguier, D. Monceau, L. Ressier, E. Andrieu, Acta Mater. 52 (18) (2004) 5375.
[12] Y. Shimomura, K. Sugio, Y. Kogure, M. Doyama, Comput. Mater. Sci. 14 (1999) 36.
[13] Y. Shimomura, Mater. Chem. Phys. 50 (1997) 139.
[14] D.J. Bacon, J. Nucl. Mater. 206 (1993) 249.
[15] M. Kiritani, J. Nucl. Mater. 276 (2000) 41.
[16] Y. Kraftmaher, Phys. Rep. 299 (1998) 79.
[17] G. Kresse, J. Hafner, Phys. Rev. B 47 (1993) 558;
G. Kresse, J. Hafner, Phys. Rev. B 49 (1994) 14251;
G. Kresse, J. Furthmüller, Phys. Rev. B 54 (1996) 11169;
G. Kresse, J. Furthmüller, Comput. Mater. Sci. 6 (1996) 15.
[18] G. Kresse, D. Joubert, Phys. Rev. B 59 (1999) 1758.
[19] Y. Wang, J.P. Perdew, Phys. Rev. B 44 (13) (1991) 298.
[20] H.J. Monkhorst, J.D. Pack, Phys. Rev. B 13 (1976) 5188.

[21] For large super-cells (128 and 250 atoms, which corresponds to $4 \times 4 \times 4$ and $5 \times 5 \times 5$ supercells), we need, by band folding, to use a $n \times n \times n$ Monkhorst–Pack meshes, where $n = 4$ and 3.2, respectively. To simplify, we thus used the same MP grid.
[22] T. Shimada, Yoshiyuki Ishii, Takayuki Kitamura, Phys. Rev. B 81 (2010) 134420.
[23] P. Blonski, A. Kiejna, J. Hafner, Phys. Rev. B 77 (2008) 155424.
[24] P. Kumar Nandi, M.C. Valsakumar, Sharat. Chandra, H.K. Sahu, C.S. Sundar, J. Phys.: Condens. Matter 22 (2010) 345501.
[25] Y. Tateyama, T. Ohno, Phys. Rev. B 67 (2003) 174105.
[26] P.A. Korzhavyi, I.A. Abrikosov, B. Johansson, A.V. Ruban, H.L. Skriver, Phys. Rev. B 59 (1999) 11693.
[27] P. Soderlind, L.H. Yang, J.A. Moriarty, J.M. Wills, Phys. Rev. B 61 (2000) 2579.
[28] C. Domain, C.S. Becquart, Phys. Rev. B 65 (2001) 024103.
[29] P. Olsson, C. Domain, J. Wallenius, Phys. Rev. B 75 (2007) 014110.
[30] C.-C. Fu, F. Willaime, P. Ordejon, Phys. Rev. Lett. 92 (2004) 175503.
[31] T. Ohnuma, N. Soneda, M. Iwasawa, Acta Mater. 57 (2009) 5947–5955.
[32] H.E. Schaefer, K. Maier, M. Weller, D. Herlach, A. Seeger, Diehl, Scr. Metall. 11 (1977) 803.
[33] H. Matter, J. Winter, W. Triftshäuser, Appl. Phys. 20 (1979) 135.
[34] S.M. Kim, W.J.L. Buyers, J. Phys. F 8 (1978) L103.
[35] K. Maier, H. Metz, D. Herlach, H.E. Schaefer, J. Nucl. Mater. 589 (1978) 69–70.
[36] L. De Schepper, D. Segers, L. Dorikens-Vanpraet, M. Dorikens, G. Knuyt, L.M. Stals, P. Moser, Phys. Rev. B 27 (1983) 5257.
[37] H.E. Schaefer, Phys. Status Solidi A 102 (1987) 47.
[38] A. Satta, F. Willaime, S. de Gironcoli, Phys. Rev. B 60 (1999) 7001.
[39] J.J. Burton, Phys. Rev. B 5 (1972) 2958.
[40] R.D. Hatcher, R. Zeller, P.H. Dederichs, Phys. Rev. B 19 (1979) 5083.
[41] S.S. Pohlong, P.N. Ram, J. Phys.: Condens. Matter 10 (1998) 10901.
[42] G. Lucas, R. Schaeublin, NIMB 267 (2009) 3009.
[43] A. Vehanen, P. Hautojarvi, J. Johansson, J. Yli-Kauppila, P. Moser, Phys. Rev. B 25 (1982) 762.
[44] C.C. Fu, J. Dalla Torre, F. Willaime, J.-L. Bocquet, A. Barbu, Nat. Mater. 4 (2005) 68.
[45] G.H. Vineyard, J. Phys. Chem. Solid 3 (1957) 121.
[46] Y.N. Osetsky, A. Serra, Defect Diffus. Forum 155 (1997) 143–147.
[47] J.C. Boettger, Phys. Rev. B 53 (1996) 13133.
[48] P. Błoński, A. Kiejna, Surf. Sci. 601 (2007) 123.
[49] M.J.S. Spencer, A. Hung, I.K. Snook, I. Yarovsky, Surf. Sci. 513 (2002) 389.
[50] P. Blonski, A. Kiejna, Vacuum 74 (2004) 179.
[51] L. Vitos, A.V. Ruban, H.L. Skriver, J. Kollar, Surf. Sci. 411 (1998) 186.
[52] H.L. Skriver, N.M. Rosengaard, Phys. Rev. B 46 (1992) 7157.
[53] W.R. Tyson, W.A. Miller, Surf. Sci. 62 (1977) 267.
[54] F.R. de Boer, R. Boom, W.C.M. Mattens, A.R. Miedema, A.K. Niessen, Cohesion in Metals, North-Holland, Amsterdam, 1988.
[55] For these simulations the slabs were reduced to seven Fe atomic layers.
[56] C.Q. Wang, Y.X. Yang, Y.S. Zhang, Y. Jia, Comput. Mater. Sci. 50 (2010) 291294.
[57] C. Wang, Z. Qin, Y. Zhang, Q. Sun, Y. Jia, Appl. Surf. Sci. 258 (2012) 4294–4300.
[58] J.R. Beeler Jr., R.A. Johnson, Phys. Rev. 156 (1967) 677.
[59] K. Masuda, Phys. Status Solidi (b) 112 (1982) 609.
[60] R.A. Johnson, D.J. Oh, J. Mater. Res. 4 (1989) 1195.
[61] F. Djurabekova, L. Malerba, R.C. Pasianot, P. Olsson, Philos. Mag. 90 (2010) 2585.
[62] C.J. Forst, J. Slycke, K.J. Van Vliet, S. Yip, Phys. Rev. Lett. 96 (2006) 175501.
[63] D. Connétable, J. Huez, E. Andrieu, C. Mijoule, J. Phys.: Condens. Matter 23 (2011) 405401.